Editors' Suggestion

Bending of Multilayer van der Waals Materials

Guorui Wang,[1,4,*] Zhaohe Dai,[2,*] Junkai Xiao,[1,*] ShiZhe Feng,[3] Chuanxin Weng,[1] Luqi Liu,[1,†] Zhiping Xu,[3,‡] Rui Huang,[2,§] and Zhong Zhang[1,4,‖]

[1]*CAS Key Laboratory of Nanosystem and Hierarchical Fabrication, CAS Center for Excellence in Nanoscience, National Center for Nanoscience and Technology, Beijing 100190, China*

[2]*Department of Aerospace Engineering and Engineering Mechanics, The University of Texas at Austin, Austin, Texas 78712, USA*

[3]*Applied Mechanics Laboratory, Department of Engineering Mechanics and Center for Nano and Micro Mechanics, Tsinghua University, Beijing 100084, China*

[4]*CAS Key Laboratory of Mechanical Behavior and Design of Materials, Department of Modern Mechanics, University of Science and Technology of China, Hefei 230026, China*

(Received 25 April 2019; published 9 September 2019)

Out-of-plane deformation patterns, such as buckling, wrinkling, scrolling, and folding, formed by multilayer van der Waals materials have recently seen a surge of interest. One crucial parameter governing these deformations is bending rigidity, on which significant controversy still exists despite extensive research for more than a decade. Here, we report direct measurements of bending rigidity of multilayer graphene, molybdenum disulfide (MoS_2), and hexagonal boron nitride (hBN) based on pressurized bubbles. By controlling the sample thickness and bubbling deflection, we observe platelike responses of the multilayers and extract both their Young's modulus and bending rigidity following a nonlinear plate theory. The measured Young's moduli show good agreement with those reported in the literature ($E_{\text{graphene}} > E_{\text{hBN}} > E_{\text{MoS}_2}$), but the bending rigidity follows an opposite trend, $D_{\text{graphene}} < D_{\text{hBN}} < D_{\text{MoS}_2}$ for multilayers with comparable thickness, in contrast to the classical plate theory, which is attributed to the interlayer shear effect in the van der Waals materials.

DOI: 10.1103/PhysRevLett.123.116101

Two-dimensional (2D) materials possess excellent electronic, mechanical, and chemical properties that lend well to a range of applications [1–3]. In many instances, 2D materials come with multilayered structures [also called multilayer van der Waals (vdW) materials] and favor out-of-plane deformations such as scrolls [4,5], folds [6–8], bubbles [9–14], wrinkles [15,16], buckles [17,18], crumples [19,20], ripples [21,22], tents [23–25], and so on due to their thinness [Figs. 1(a) and 1(b)]. On the one hand, the out-of-plane mode of deformation is viewed as an inconvenience, with research focusing on how it might be avoided [26]. On the other hand, the development of 2D-material-based stretchable electronics and strained semiconductors can take advantage of these curved configurations [27,28]. For these purposes, it is often necessary to manipulate and control the out-of-plane deformation of multilayer 2D materials, which requires understanding the mechanics and underlying mechanisms of bending these atomically layered structures, where in particular, the bending rigidity is deemed as one crucial parameter [29].

Classical plate theory assumed that an elastic plate resists bending by tension and compression on the opposite sides of a neutral plane [30]. The bending rigidity of an elastic plate is related to its thickness (t) and the elastic moduli of the material by $D = Et^3/12(1-\nu^2)$, where E is Young's modulus and ν is Poisson's ratio. This relation holds well for a perfectly glued multilayer with N identical layers [Fig. 1(c)] such that the overall bending rigidity D is proportional to N^3. However, the classical relation is expected to break down for multilayer 2D materials for at least two reasons. (i) The mechanical resistance of the monolayer 2D material to bending and stretching deformation arises from different physical origins [31–34]. In graphene, for example, the Young's modulus is related to the in-plane σ bonding, while the bending resistance is attributed to the distortion of out-of-plane π bonds [31]. (ii) The vdW interactions between the atomic layers are weak in resisting interlayer shear or sliding [35,36], as demonstrated by recently observed self-rotation between 2D material layers [37,38]. The interlayer shear stiffness and strength of bulk 2D materials (e.g., graphite) is typically orders of magnitude lower than their in-plane Young's modulus and tensile strength [39]. This extreme mechanical anisotropy may subject multilayer 2D materials to the interlayer sliding. In the limiting case when the interface is ultralubricated [Fig. 1(d)], each layer would bend independently such that the overall bending rigidity of the multilayer would scale linearly with the number of layers, $D \sim N$.

Despite extensive research into the mechanical properties of 2D materials for more than a decade, significant

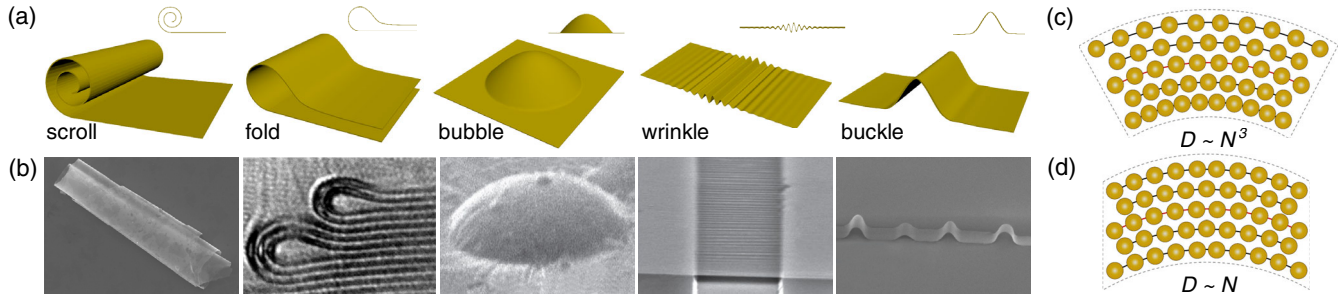

FIG. 1. The schematics (a) and corresponding electron microscope images (b) illustrate various deformation modes. (Reproduced with permission from Refs. [4,8,14,15,17]). Panels (c) and (d) illustrate the microstructural deformation upon bending of multilayer 2D materials with perfectly glued (c) and ultralubricated (d) interfaces.

controversy still exists on the bending rigidity of monolayer and multilayer 2D materials [15,21,31,34]. It remains elusive how the bending rigidity of a multilayer 2D material relates to its layer number, although the classical relation ($D \sim N^3$) has been widely applied in the literature despite the perceived breakdown. Motivated by this puzzle, here we focus on experimentally measuring the bending rigidity of multilayer 2D materials through pressurized bubble devices. Graphene, hexagonal boron nitride (hBN), and molybdenum disulfide (MoS_2) are chosen as representatives of metallic, insulating, and semiconducting 2D materials, respectively. The effect of interlayer coupling on the bending rigidity of 2D materials is revealed.

Figure 2 illustrates the pressurized bubble device that can create axisymmetric out-of-plane deformation of 2D materials. The samples are made by mechanical exfoliation of multilayer graphene, hBN, and MoS_2 over patterned holes (radius: 0.5–1.5 μm) on a SiO_2/Si substrate. The number of layers (N) in these multilayers, ranging from 7 to 70 [40], can be identified by atomic force microscopy (AFM) and Raman spectroscopy. Following the well-developed gas diffusion procedure [12,40], we can apply a pressure difference (Δp) across the multilayer and bulge upwards in a controllable manner. The height profile of each bubble is then measured by AFM.

We first observe the shape characteristics of 2D material bubbles. Classical theory predicts the deflection of a plate responding to a uniform pressure as follows:

$$\frac{w(r)}{h} = \left(1 - \frac{r^2}{a^2}\right)^{\alpha} \tag{1}$$

where $w(r)$ is the out-of-plane deflection profile, h is the bubble height (deflection at the center), r is the distance from the hole center, a is the hole radius, and the exponent α is 2 for a linear elastic plate. However, such a platelike profile is rarely observed in 2D material bubbles because of the extreme thinness and flexibility of 2D materials [9–13]. Alternatively, the membrane limit is commonly adopted for these 2D material bubbles, where the bending rigidity is assumed to be negligible and the deflection profile of the bubble is approximately taken as a spherical cap, i.e., $\alpha = 1$ in Eq. (1) [9–13]. The membrane analysis has been adopted to measure fundamental mechanical properties of 2D materials [9–13] such as Young's modulus, interfacial adhesion and friction, and electromechanical coupling, but not for bending rigidity.

We show in Fig. 2(b) experimentally measured profiles from graphene bubbles with a variety of thicknesses and heights. We normalize the deflection by the bubble height and the radial position by the bubble radius. For bubbles with radii of 0.5 μm, the normalized deflection profiles collapse onto one curve as predicted by the membrane analysis when the ratio between the bubble height and the thickness of the multilayer, h/t, is larger than 2—the case of most previous works [9–13]. For bubbles with the height comparable to the thickness, i.e., $h/t \lesssim 1.5$, the bending

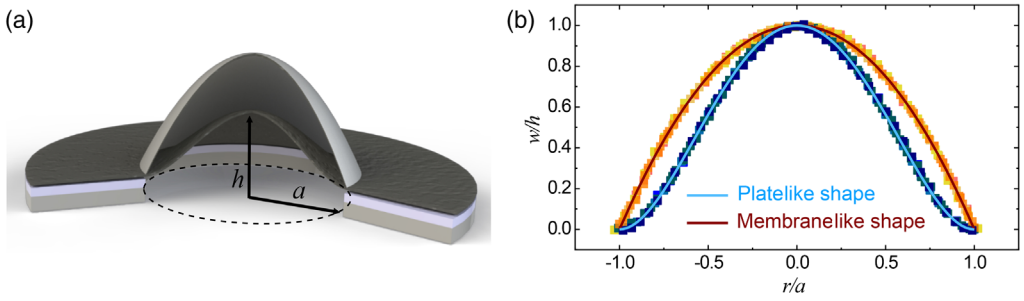

FIG. 2. (a) The schematic of pressurized bubbles with two distinct shape characteristics at small and large deflections. (b) Normalized deflection profiles measured from two sets of 0.5-μm-radius bubbles. We observe a membranelike shape with a kinked edge for $h/t \gtrsim 2$ (orange markers) and a platelike shape with a smooth edge for $h/t \lesssim 1.5$ (blue markers).

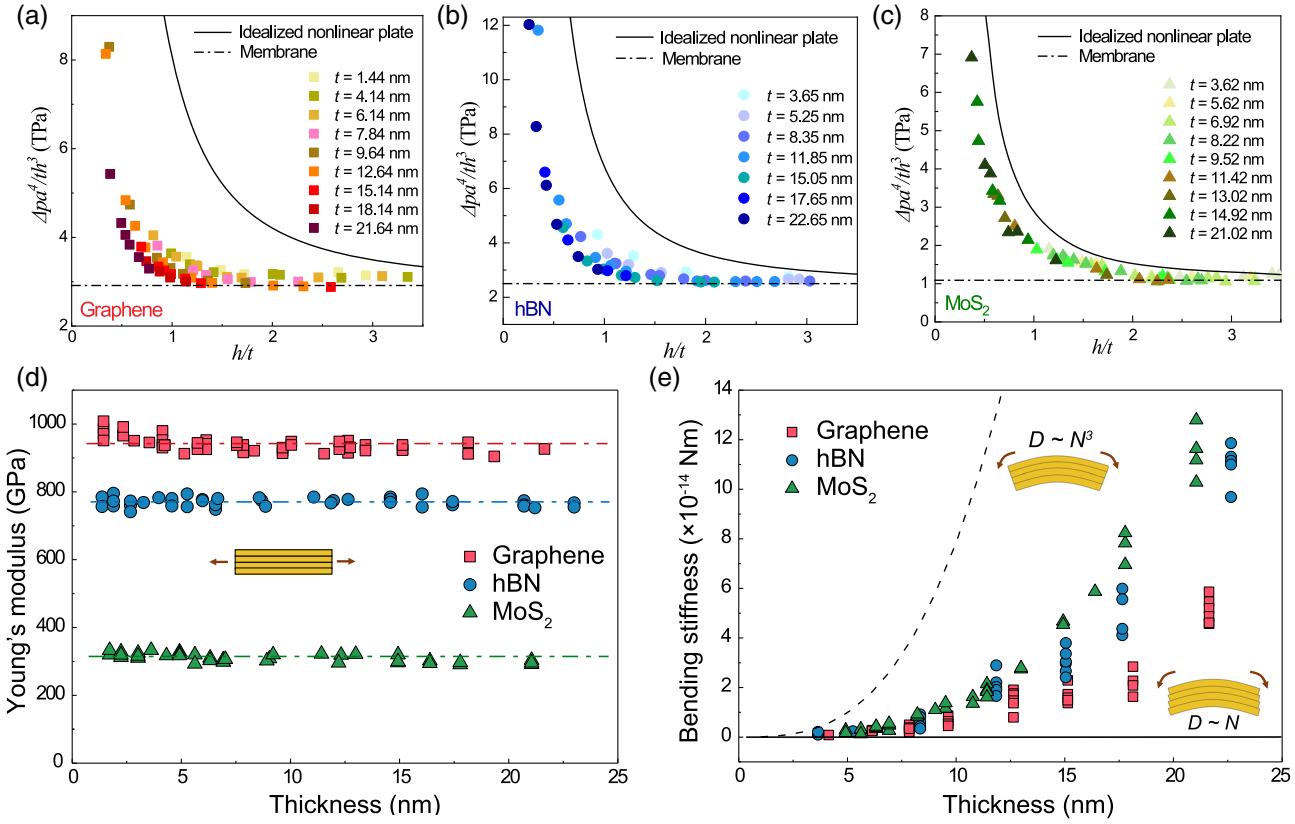

FIG. 3. We show $\Delta pa^4/h^3t$ as a function of h/t for graphene (a), hBN (b) and MoS_2 (c), respectively. The solid lines represent the idealized nonlinear plate solution, and horizontal dot-dashed lines are the membrane solution. In the color system, the darker symbol denotes the thicker sample. Extracted Young's modulus (d) and bending rigidity (e) as a function of thickness. At a given thickness, AFM measurements of up to 17 different bubbles produce the results plotted as symbols. The dash-dotted lines in (d) indicate the average values, while the dashed and solid lines in (e) are the theoretical predictions for the perfectly glued ($D \sim N^3$) and ultralubricated ($D \sim N$) cases, respectively.

effect becomes significant so that the deflection profiles collapse onto a different curve predicted by the plate theory. This observation implies that membranelike behavior can transit to platelike behavior for the bubbles of multilayer 2D materials by simply tuning the ratio h/t. The membrane-to-plate transition also makes it possible to simultaneously determine the in-plane Young's modulus and bending rigidity of the 2D multilayers. We note that the critical h/t for such transition depends on the bubble radius and also varies slightly from material to material (Fig. S5 [40]).

We then consider the pressure-height relation for these multilayer 2D material bubbles. Previous numerical studies proposed a nonlinear plate analysis for pressurized bubbles that included both in-plane stretching and bending of the 2D material, leading to [54,55]

$$\frac{\Delta pa^4}{h^3t} = A(\nu)E + \frac{64D}{t^3}\left(\frac{t}{h}\right)^2 \tag{2}$$

where $A(\nu) \simeq (0.7179 - 0.1706\nu - 0.1495\nu^2)^{-3}$, which is 3.10 for graphene with $\nu = 0.165$, 3.28 for hBN with $\nu = 0.221$, and 3.46 for MoS_2 with $\nu = 0.27$ [56]. Note that Eq. (2) was found to be a good approximation even for monolayer graphene bubbles by using the 2D in-plane stiffness ($E_{2D} = Et$) and a bending rigidity (D) that is independent of E [54]. We also note that the interfacial shear deformation between the supported 2D material and the SiO_2 substrate is negligible in our experiments because of the relatively small pressure and deflection [Figs. S4(d)—S4(f)], and hence the clamped boundary condition at the edge of the bubble is reasonable. In Figs. 3(a)–3(c), the dot-dashed lines represent the membrane limit of Eq. (2) where the bending term is neglected. The solid lines represent the idealized nonlinear plate model assuming a bending rigidity $D = Et^3/12(1-\nu^2)$ such that the response $[(\Delta pa^4/h^3t)\text{vs.}h/t]$ does not depend on the thickness. Evidently, the experimentally measured responses for all three 2D materials approach the membrane limit when the ratio h/t is greater than 2. For $h/t < 1.5$, the bubble responses exhibit a transition to the platelike behavior but deviate considerably from the idealized nonlinear plate solution. This observation implies that the use of the classical $D - E$ relation would overestimate the bending rigidity of the multilayer 2D materials. Moreover, the effect of pretension is found to be negligible in our experiments, as measured responses $[(\Delta pa^4/h^3t)\text{vs.}h/t]$ for our samples

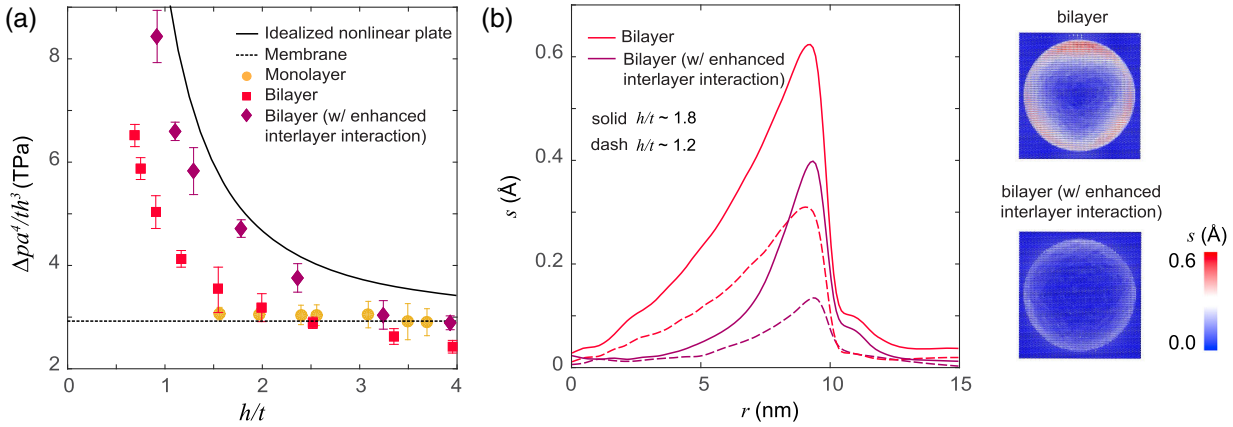

FIG. 4. (a) The mechanical response of monolayer and bilayer graphene bubbles to pressure in MD simulations. The solid line represents the idealized nonlinear plate solution, while the dashed line is the membrane solution. For bilayer samples, a stronger resistance to pressure is observed by enhancing the interlayer interaction strength. The error bars are from thermal fluctuations in MD simulations. (b) Radial distribution of the atomic slip length (s) in the bulged bilayer graphene with the height-thickness ratio h/t of ~1.2 and 1.8, respectively. The right panel of (b) shows the area distribution of s for bilayer graphene with h/t of ~1.2. Enhancing the strength of interlayer interactions can restrain interlayer sliding, leading to reduced slip lengths and higher bending rigidity.

with different radii also collapse onto the radius-independent curve as predicted by Eq. (2) (Fig. S6 [40]).

Equation (2) allows us to determine both Young's modulus and bending rigidity of the multilayer 2D material as well as their dependency on the layer thickness. We start with Young's moduli of multilayer 2D materials by focusing on samples under relatively large pressure [55]. In this case, h/t is relatively large, and the second term on the right-hand side of Eq. (2) is negligible (the membrane limit); thus Young's modulus can be determined directly by measuring $\Delta pa^4/h^3t$. In Figs. 3(a)–3(c), for graphene, hBN, and MoS_2 bubbles with $h/t \gtrsim 2$, the data for $\Delta pa^4/h^3t$ collapse onto the dot-dashed lines, as predicted by the membrane limit. The domain of h/t for the membranelike behavior is consistent with our shape measurements in Fig. 2. We then extract Young's moduli of the multilayer 2D materials as summarized in Fig. 3(d). We find that the average values are 939.5 ± 21.7 GPa, 769.9 ± 12.9 GPa, and 314.3 ± 8.4 GPa for the multilayer graphene, hBN, and MoS_2 with layer numbers ranging from about 10 to 70. For each 2D material, the extracted Young's modulus shows essentially no dependency on the thickness, and the average values agree well with those measured by AFM indentation of monolayers [56–58].

When the height of the deformed bubble becomes comparable to the thickness of 2D multilayers, the contribution from bending is substantiated, and both terms on the right-hand side of Eq. (2) should be accounted for. A membrane-to-plate transition is expected to occur in the mechanical response of bubbles (Fig. 2). With the thickness-independent Young's modulus extracted from the membrane model, we can then calculate the bending rigidity D by comparing Eq. (2) with the measured response $\Delta pa^4/h^3t$ for bubbles with relatively small deflection ($h/t \lesssim 1.5$) (Fig. S5 [40]). Figure 3(e) summarizes the values of D for graphene, hBN, and MoS_2 multilayers, and the possible errors for these measurements are discussed in Fig. S3 [40]. As expected, the bending rigidity increases with the thickness of 2D materials. However, the thickness dependence does not follow either one of the two limiting cases. Specifically, the bending rigidity of a multilayer graphene ($t > 5$ nm) is much lower than that expected from classical plate theory [$D \sim t^3$; dashed line in Fig. 3(e)] but much higher than the ideally lubricated cases [$D \sim t$; solid line in Fig. 3(e)]. More interestingly, for samples with similar thickness, we find $D_{MoS_2} > D_{hBN} > D_{graphene}$, whereas the values of Young's moduli are ordered inversely, that is, $E_{graphene} > E_{hBN} > E_{MoS_2}$. This again indicates that the bending rigidity of multilayer 2D materials violates the predictions of the classical plate theory.

We attribute the abnormal bending behaviors of multilayer 2D materials to the effect of interlayer shear or slippage between atomic sheets, which breaks down the assumptions in classical plate theory. The interlayer sliding of 2D material bilayers has been reported by detailed first-principles analysis in the literature where interfacial shear strengths were proposed to capture the sliding capability [59–61]. To further elucidate the interaction between the interlayer sliding and in-plane elasticity, we carry out molecular dynamics (MD) simulations of gas-pressurized circular graphene bubbles [40]. We plot the mechanical responses of monolayer and bilayer graphene bubbles to pressure in Fig. 4(a), along with the predictions by Eq. (2) for the plate and membrane solutions. We find that, for monolayers, the bending rigidity is negligible [31], and a Young's modulus of ~1 TPa can be deduced from the membrane analysis of the MD results, validating our simulation setups. We then focus on bilayer graphene bubbles, especially at small deflections (i.e., $h/t < \sim 1.5$) where the effect of bending rigidity is noticeable. Our simulation

results align well with experimental data in Fig. 3(a)—both are overestimated by the idealized nonlinear plate solution [solid line in Fig. 4(a)] where the classical $D-E$ relation is used. Remarkably, the MD simulations show that the mechanical response of bilayer graphene bubbles depends on the interlayer potential parameters. In particular, the bending rigidity of the bilayer graphene is effectively enhanced when the strength of the interlayer interaction is increased in the MD simulations.

To further shed light on the interlayer shear or slippage deformations, we define an atomic slip length, s, for the atoms in the top graphene sheet in the bilayer to identify the local shear or sliding between the top and bottom lattices [40]. In perfect AB stacking, the value of s is zero for all atoms. As the bilayer structure is pressurized into bubbles, interlayer slippage at the center of the bubble is absent due to the symmetry. However, the value of s becomes nontrivial and increases along the radial direction, reaching the maximum at the edge of the bilayer graphene bubble [dashed lines in Fig. 4(b)]. As expected, the slip length can be further actuated by increasing the deflection of the bubble. Notably, such interlayer slippage can be significantly reduced by enhancing the strength of interlayer interactions as shown in Fig. 4(b). Combining with the simulated mechanical resistance of graphene bilayer bubbles summarized in Fig. 4(a), we conclude that the interlayer shear or slippage between 2D materials competes with intralayer deformation (stretching and bending) and can modulate the overall mechanical responses. Clearly, such an effect is absent in the classical plate theory, which essentially assumes no interlayer slippage.

Both our experiments and MD simulations show that the classical relation for the bending rigidity, $D=Et^3/12(1-\nu^2)$, in general, is not valid for multilayer 2D materials, where the interlayer shear interactions are weak and slippage is inevitable. This mechanism may be qualitatively simple to understand, but the quantitative measurement of its effect on the bending properties of a 2D material multilayer has been challenging and has not been reported, to the best of our knowledge. To account for such effects, we propose a modified formula for the effective bending rigidity of multilayer 2D materials as

$$D_{\mathrm{eff}}=f(N)\frac{Et^3}{12(1-\nu^2)} \tag{3}$$

where $f(N)$ is a function of the layer number and it depends on the strength of interlayer shear interactions, as a result of competition between the intralayer stretching or compressing and the interlayer shear or sliding. Theoretically, there are two limiting cases. The upper bound assumes perfect bonding so that the interlayer slippage is prohibited [Fig. 1(c)], while the lower bound corresponds to frictionless interlayer interactions or ultralubricated [Fig. 1(d)].

In Fig. 5, we plot the two limits by solid lines using the parameters of graphene; the limits for hBN and MoS_2 are slightly different [40]. Experimentally, the function $f(N)$ can be determined based on Eq. (2): $f(N)=[3(1-v^2)h^2/16t^2][(\Delta pa^4/Eth^3)-A(\nu)]$, as shown in Fig. 5 for multilayer graphene, hBN, and MoS_2 (also in Fig. S8 [40]). Evidently, the values of $f(N)$ for these multilayer 2D materials lie between the two theoretical limits. These results imply that both intralayer stretching or compressing and the interlayer shear or sliding happen when bending the multilayer 2D materials. Among the three 2D materials, the graphene multilayers have the lowest values of $f(N)$, and the MoS_2 multilayers have the highest value. Despite the highest in-plane elastic modulus of graphene, the bending rigidity of multilayer graphene is the lowest due to the interlayer slippage, close to the lower limit. This result can also be quantitatively explained by a decomposition of the simulated deformation of pressurized bilayer graphene (see details in Note 4.3 [40]). It is expected that the modified formula for the bending rigidity in Eq. (3) not only works very well for all our samples (see Fig. S9 [40]) but also applies, more broadly, for other multilayer vdW materials and their homostructures or heterostructures. The methods and data provided in this work offer quantitative measures for the elastic responses of multilayer 2D materials through a simple function $f(N)$. This function may quantify the level of interlayer slippage, as well as the coupling between stretching and bending, which highly depend on the types of 2D materials [46–48] and its multilayer structures.

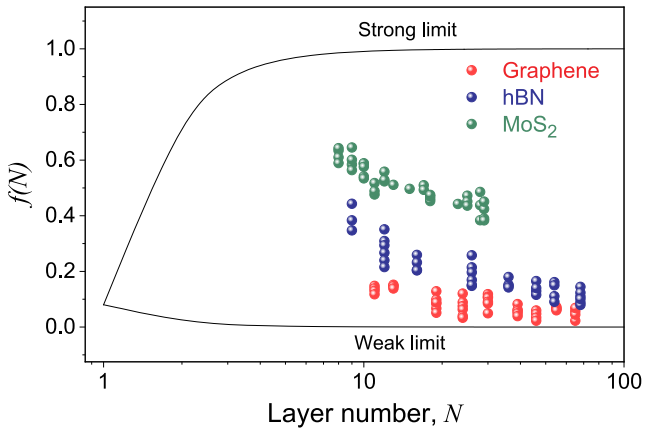

FIG. 5. The layer-dependent function to measure the effect of interlayer coupling on the bending rigidity of multilayered graphene, hBN, and MoS_2. The black lines are theoretical predictions of the limiting cases for graphene. Our experimental results are denoted by colored markers, sitting between the two limits.

This work is jointly supported by National Natural Science Foundation of China (Grants No. 11890682, No. 11832010, No. 21474023, and No. 21721002), the Strategic Priority Research Program of CAS under Grant No. XDB30020100, the National Key Basic Research Program of China (Grant No. 2013CB934203), and the National Key Research and Development Program of China (Grant No. 2016YFA0301204).

*These authors contributed equally to this work.
†Correspondence author.
liulq@nanoctr.cn
‡Correspondence author.
xuzp@tsinghua.edu.cn
§Correspondence author.
ruihuang@mail.utexas.edu
‖Correspondence author.
zhong.zhang@nanoctr.cn.

[1] A. K. Geim and I. V. Grigorieva, Nature (London) **499**, 419 (2013).
[2] K. S. Novoselov, A. Mishchenko, A. Carvalho, and A. H. Castro Neto, Science **353**, aac9439 (2016).
[3] P. H. Tan *et al.*, Nat. Mater. **11**, 294 (2012).
[4] X. Zhang, S. Liu, and X. Shao, J. Lumin. **136**, 32 (2013).
[5] X. Cui, Z. Kong, E. Gao, D. Huang, Y. Hao, H. Shen, C.-a. Di, Z. Xu, J. Zheng, and D. Zhu, Nat. Commun. **9**, 1301 (2018).
[6] J. Annett and G. L. Cross, Nature (London) **535**, 271 (2016).
[7] J. Zhao, Q. Deng, T. H. Ly, G. Han, G. Sandeep, and M. H. Rummeli, Nat. Commun. **6**, 8935 (2015).
[8] A. Lopez-Bezanilla *et al.*, J. Phys. Chem. Lett. **3**, 2097 (2012).
[9] N. Levy, S. Burke, K. Meaker, M. Panlasigui, A. Zettl, F. Guinea, A. C. Neto, and M. Crommie, Science **329**, 544 (2010).
[10] G. Wang, Z. Dai, Y. Wang, P. H. Tan, L. Liu, Z. Xu, Y. Wei, R. Huang, and Z. Zhang, Phys. Rev. Lett. **119**, 036101 (2017).
[11] D. A. Sanchez, Z. Dai, P. Wang, A. Cantu-Chavez, C. J. Brennan, R. Huang, and N. Lu, Proc. Natl. Acad. Sci. U.S.A. **115**, 7884 (2018).
[12] S. P. Koenig, N. G. Boddeti, M. L. Dunn, and J. S. Bunch, Nat. Nanotechnol. **6**, 543 (2011).
[13] E. Khestanova, F. Guinea, L. Fumagalli, A. K. Geim, and I. V. Grigorieva, Nat. Commun. **7**, 12587 (2016).
[14] J. Lee, X. Zheng, R. C. Roberts, and P. X.-L. Feng, Diamond Relat. Mater. **54**, 64 (2015).
[15] W. Bao, F. Miao, Z. Chen, H. Zhang, W. Jang, C. Dames, and C. N. Lau, Nat. Nanotechnol. **4**, 562 (2009).
[16] Z. Dai, L. Liu, and Z. Zhang, Adv. Mater. 1805417 (2019).
[17] S. Yang *et al.*, Nano Lett. **15**, 1660 (2015).
[18] A. Castellanos-Gomez, R. Roldan, E. Cappelluti, M. Buscema, F. Guinea, H. S. van der Zant, and G. A. Steele, Nano Lett. **13**, 5361 (2013).
[19] J. Zang, S. Ryu, N. Pugno, Q. Wang, Q. Tu, M. J. Buehler, and X. Zhao, Nat. Mater. **12**, 321 (2013).
[20] P. Chen, J. Sodhi, Y. Qiu, T. M. Valentin, R. S. Steinberg, Z. Wang, R. H. Hurt, and I. Y. Wong, Adv. Mater. **28**, 3564 (2016).
[21] L. Tapaszto, T. Dumitrica, S. J. Kim, P. Nemes-Incze, C. Hwang, and L. P. Biro, Nat. Phys. **8**, 739 (2012).
[22] S. Xie *et al.*, Science **359**, 1131 (2018).
[23] A. Reserbat-Plantey *et al.*, Nano Lett. **14**, 5044 (2014).
[24] Y. Jiang, J. Mao, J. Duan, X. Lai, K. Watanabe, T. Taniguchi, and E. Y. Andrei, Nano Lett. **17**, 2839 (2017).
[25] Z. Dai, Y. Hou, D. A. Sanchez, G. Wang, C. J. Brennan, Z. Zhang, L. Liu, and N. Lu, Phys. Rev. Lett. **121**, 266101 (2018).
[26] F. Pizzocchero, L. Gammelgaard, B. S. Jessen, J. M. Caridad, L. Wang, J. Hone, P. Boggild, and T. J. Booth, Nat. Commun. **7**, 11894 (2016).
[27] F. De Juan, A. Cortijo, M. A. Vozmediano, and A. Cano, Nat. Phys. **7**, 810 (2011).
[28] F. Guinea, M. I. Katsnelson, and A. K. Geim, Nat. Phys. **6**, 30 (2010).
[29] M. K. Blees *et al.*, Nature (London) **524**, 204 (2015).
[30] S. P. Timoshenko and S. Woinowsky-Krieger, *Theory of Plates and Shells* (McGraw-Hill, New York, 1959).
[31] D. B. Zhang, E. Akatyeva, and T. Dumitrica, Phys. Rev. Lett. **106**, 255503 (2011).
[32] Y. Wei, B. Wang, J. Wu, R. Yang, and M. L. Dunn, Nano Lett. **13**, 26 (2013).
[33] Q. Lu, M. Arroyo, and R. Huang, J. Phys. D **42**, 102002 (2009).
[34] M. Zelisko, F. Ahmadpoor, H. Gao, and P. Sharma, Phys. Rev. Lett. **119**, 068002 (2017).
[35] O. Hod, E. Meyer, Q. Zheng, and M. Urbakh, Nature (London) **563**, 485 (2018).
[36] R. Ribeiro-Palau, C. J. Zhang, K. Watanabe, T. Taniguchi, J. Hone, and C. R. Dean, Science **361**, 690 (2018).
[37] D. Wang *et al.*, Phys. Rev. Lett. **116**, 126101 (2016).
[38] C. Woods *et al.*, Nat. Commun. **7**, 10800 (2016).
[39] B. T. Kelly, *Physics of Graphite* (Applied Science, London, 1981).
[40] See Supplemental Material at http://link.aps.org/supplemental/10.1103/PhysRevLett.123.116101 for experimental setup and characterizations, identification of the membrane-plate transition and molecular dynamics simulations, which includes Refs. [41–53].
[41] H. Li, J. Wu, X. Huang, G. Lu, J. Yang, X. Lu, Q. Xiong, and H. Zhang, ACS Nano **7**, 10344 (2013).
[42] X. Li, X. Qiao, W. Han, Y. Lu, Q. Tan, X. Liu, and P. Tan, Nanoscale **7**, 8135 (2015).
[43] L. Li, J. Cervenka, K. Watanabe, T. Taniguchi, and Y. Chen, ACS Nano **8**, 1457 (2014).
[44] C. Lee, H. Yan, L. E. Brus, T. F. Heinz, J. Hone, and S. Ryu, ACS Nano **4**, 2695 (2010).
[45] Z. Lu and M. L. Dunn, J. Appl. Phys. **107**, 044301 (2010).
[46] S. Plimpton, J. Comput. Phys. **117**, 1 (1995).
[47] S. J. Stuart, A. B. Tutein, and J. A. Harrison, J. Chem. Phys. **112**, 6472 (2000).
[48] Z. Xu, J. Comput. Theor. Nanosci. **6**, 625 (2009).
[49] A. N. Kolmogorov and V. H. Crespi, Phys. Rev. B **71**, 235415 (2005).
[50] P. Espanol and P. B. Warren, J. Chem. Phys. **146**, 150901 (2017).
[51] E. Gao and Z. Xu, J. Appl. Mech. **82**, 121012 (2015).
[52] W. Gao and R. Huang, J. Phys. D **44**, 452001 (2011).
[53] K. N. Kudin, G. E. Scuseria, and B. I. Yakobson, Phys. Rev. B **64**, 235406 (2001).
[54] P. Wang, W. Gao, Z. Y. Cao, K. M. Liechti, and R. Huang, J. Appl. Mech. **80**, 040905 (2013).

[55] E. H. Mansfield, *The Bending and Stretching of Plates* (Cambridge University Press, Cambridge, England, 2005).
[56] S. Bertolazzi, J. Brivio, and A. Kis, ACS Nano **5**, 9703 (2011).
[57] C. Lee, X. Wei, J. W. Kysar, and J. Hone, Science **321**, 385 (2008).
[58] S. M. Kim *et al.*, Nat. Commun. **6**, 8662 (2015).
[59] G. Levita, A. Cavaleiro, E. Molinari, T. Polcar, and M. C. Righi, J. Phys. Chem. C **118**, 13809 (2014).
[60] G. Levita, E. Molinari, T. Polcar, and M. C. Righi, Phys. Rev. B **92**, 085434 (2015).
[61] M. Wolloch, G. Levita, P. Restuccia, and M. C. Righi, Phys. Rev. Lett. **121**, 026804 (2018).